Pergamon

Journal of Structural Geology, Vol. 18, No. 6, pp. 847 to 858, 1996
Copyright © 1996 Elsevier Science Ltd
Printed in Great Britain. All rights reserved
0191-8141/96 $15.00 + 0.00

PII: S0191-8141(96)00004-1

Direct observation of deformation processes in crystal mushes

Y. PARK and W. D. MEANS

Department of Geological Sciences, University at Albany, Albany, NY 12222, U.S.A.

(*Received* 9 *May* 1995; *accepted in revised form* 6 *January* 1996)

Abstract—Isothermal microstructural development in deforming, melt-bearing crystal mushes is studied using synkinematic microscopy and a polyphase, thiocyanate system. The aim of the work is to contribute to the basis for understanding the origin of microstructures in rocks which have undergone melt-present deformation. During high strain rate, pure shearing experiments, microstructures indicating crystal plasticity and dynamic recrystallization are observed. During low strain rate, pure shearing experiments, a pressure solution-like process called *contact melting* is active, resulting in optically strain-free crystals. Crystal boundary sliding is active in both regimes. Framework scale processes such as filter pressing, grain flow, and development of a micro shear zone are illustrated. Some of these processes are cryptic microstructurally, and may be difficult or impossible to recognize in rocks. The validity of the experimental system as an analog for magmatic systems is discussed. We conclude that the experiments can serve as a source of ideas to test against the evidence from rocks, but that no direct analogy to the behavior of natural crystal mushes has been, or will readily be, established. Copyright © 1996 Elsevier Science Ltd

INTRODUCTION

Understanding melt-present deformation processes is necessary for understanding some types of igneous petrogenesis and for accurate reconstruction of structural history in areas where igneous activity occurred during regional deformation (e.g. Hutton 1988a, Paterson *et al.* 1989, Tobisch *et al.* 1989, Nicolas 1990, Bedard 1991, Karlstrom *et al.* 1993). Although significant progress has recently been made by petrographic and experimental studies (e.g. van der Molen & Paterson 1979, Cooper & Kohlstedt 1986, Dell'Angelo *et al.* 1987, Hibbard 1987), and many grain-scale deformation processes have been inferred to operate in deforming, melt-bearing mushes, direct observation of such processes has not previously been undertaken. The present experiments using synkinematic microscopy (microscopy during deformation) on non-geological crystal mushes were intended, first to observe the processes that operate in a particular crystal/melt system, and second to see what the microstructural signatures of the processes are. Although direct observation of microstructural evolution in experiments like these helps define the processes that are active in the material, we emphasize at the outset that different processes in nature might give rise to similar microstructures.

EXPERIMENTS

The experimental apparatus and sample assembly are shown in Fig. 1. The sample is a thin film of material between two glass slides (Fig. 1a). Scratches are made on the sample-facing surfaces of the slides so that thicker crystals can grow from the melt into the scratches and serve as grips to load the observed part of the sample (Fig. 1a). The scratch geometries used in this work are for pure shearing, simple shearing and general shearing (Fig. 1b). The experimental apparatus (Fig. 1c) is made of three parts: (1) a miniature press that mounts on the stage of a microscope (designed by Janos Urai, see Means 1989, Fig. 4a), (2) a heating unit and thermocontroller which can be programmed for different thermal histories, and (3) a part for recording, including a 35 mm camera, or video camera connected to a Macintosh computer with image grabber.

Sample strain rates used in these experiments range from 10% shortening (or shearing) per hour to 10% shortening per day ($10^{-4.5} \sim 10^{-6}$ s^{-1}), depending on the motor speed and width of sample between the grips. *Local strain rates* in the areas observed were commonly one or even two orders of magnitude higher than the sample strain rates, on account of uneven distribution of strain rate over the samples (i.e. high strain rate zones), and the fact that we tended to make observations in such zones. Further details of methods of synkinematic microscopy are given in Means (1989) and Ten Brink & Passchier (1995).

The crystal–melt mixture consists of two or three crystalline phases and liquid (Figs. 2a and 4a). The three crystalline phases are ammonium thiocyanate (white phase hereafter), diammonia tetrathiocyanato cobaltate (blue phase hereafter), and ammonium chloride (cube phase hereafter). The liquid phase is a hydrous solution containing various ions or ionic compounds such as NH_4^+, SCN^-, Cl^- and $(SCN)_4Co^{2-}$. The color of the liquid varies from pale to darker blue depending on the concentration of the dissolved blue phase. Known and inferred properties of solid and liquid phases are summarized in Table 1. Although the phase relations in this system are not precisely known, the phase diagram of the system seems to be of quaternary eutectic type based on crystallization and melting experiments, the four phase components being the white phase, the blue

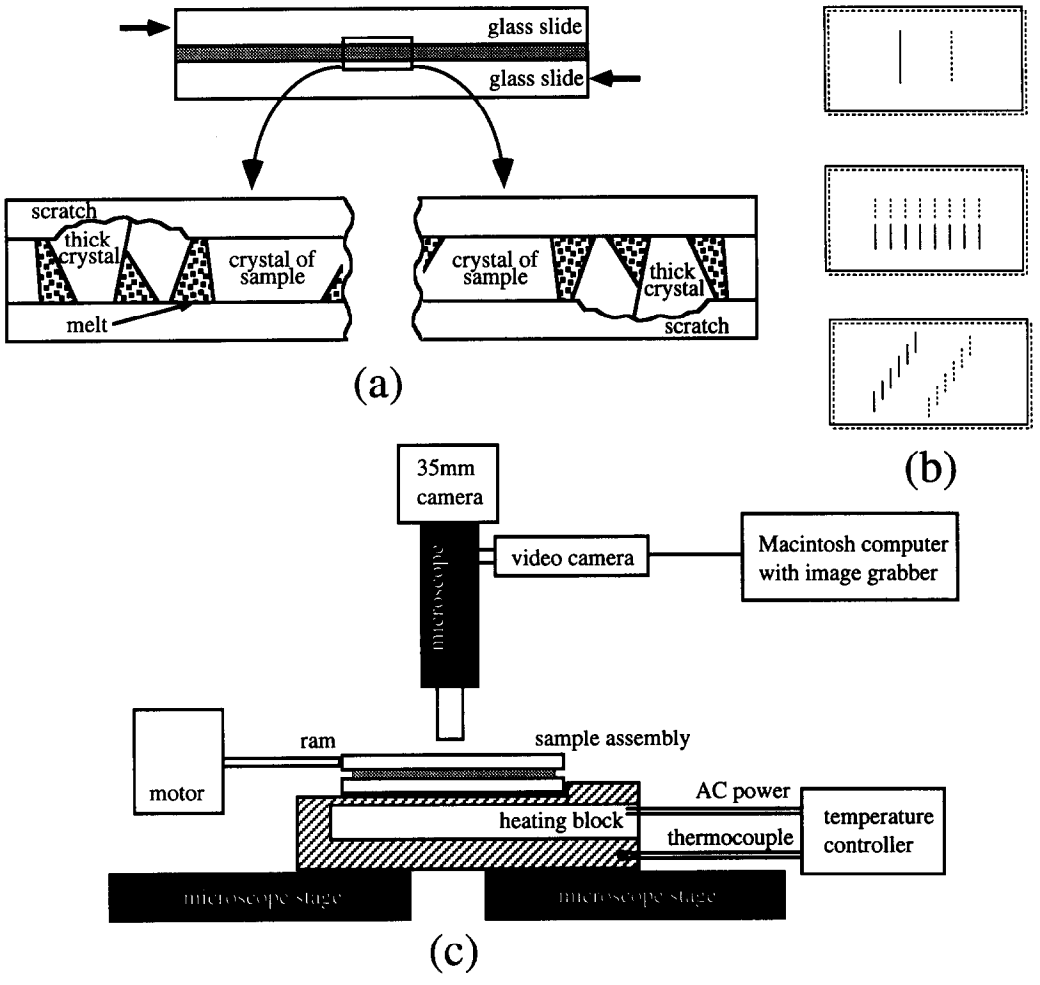

Fig. 1. Sample assembly and apparatus. (a) Two glass slides and thin film of crystal melt mixture (shaded, thickness exaggerated). Arrows indicate relative movement of slides. Scratches (grips) on glass engage thick crystals of the sample which serve to load the rest of the sample. (b) Arrangement of scratches for pure shearing, simple shearing and general shearing (top to bottom). Solid and dashed lines represent upper and lower glass slides, respectively. Slides are standard petrographic slides, 46mm in length. (c) Experimental apparatus.

phase, the cube phase, and ice. Preparation of the starting material is described in Means & Park (1994) and Park (1994).

The initial melt fraction in the samples varies from experiment to experiment ($\sim$5% to $\sim$50%) depending on the details of sample preparation. Samples with melt fractions low enough to provide a solid framework structure were used in these experiments, since interactions among crystals are essential for distributed deformation using our type of apparatus. During the volume-decreasing, pure shearing experiments described below, the melt was free to leave the samples laterally, either by moving between the grains of the sample or by moving between the sample and the glass slides.

The samples are typically only one grain thick, and about as thick as an ordinary thin section of rock, or up to about twice this thickness (e.g. 50 microns). The grain boundaries and crystal/melt boundaries lie mostly at a high angle to the plane of the glass, so they are well resolved, even in the video images that illustrate this paper. The images shown here are drawn from only five experiments, but they represent similar (though often less photogenic or unrecorded) results obtained from about thirty other deformation experiments. In all the plain light images, the contrast between crystals and melt has been enhanced somewhat, using photo manipulation software.

CRYSTAL SCALE DEFORMATION PROCESSES

Crystal plastic deformation and dynamic recrystallization

Extensive crystal plasticity and concurrent dynamic recrystallization are observed in the white phase during experiments at higher sample strain rates ($> 10^{-5}$ s^{-1}). The photomicrographs in Fig. 2 were taken during an experiment at 30° C and sample strain rate of 3×10^{-5} s^{-1}. Pure shearing grips were used, with the shortening direction parallel to the width of the photomicrographs. About 38% shortening between (a) and (b) is indicated by the lower dashed line in Fig. 2, which connects the

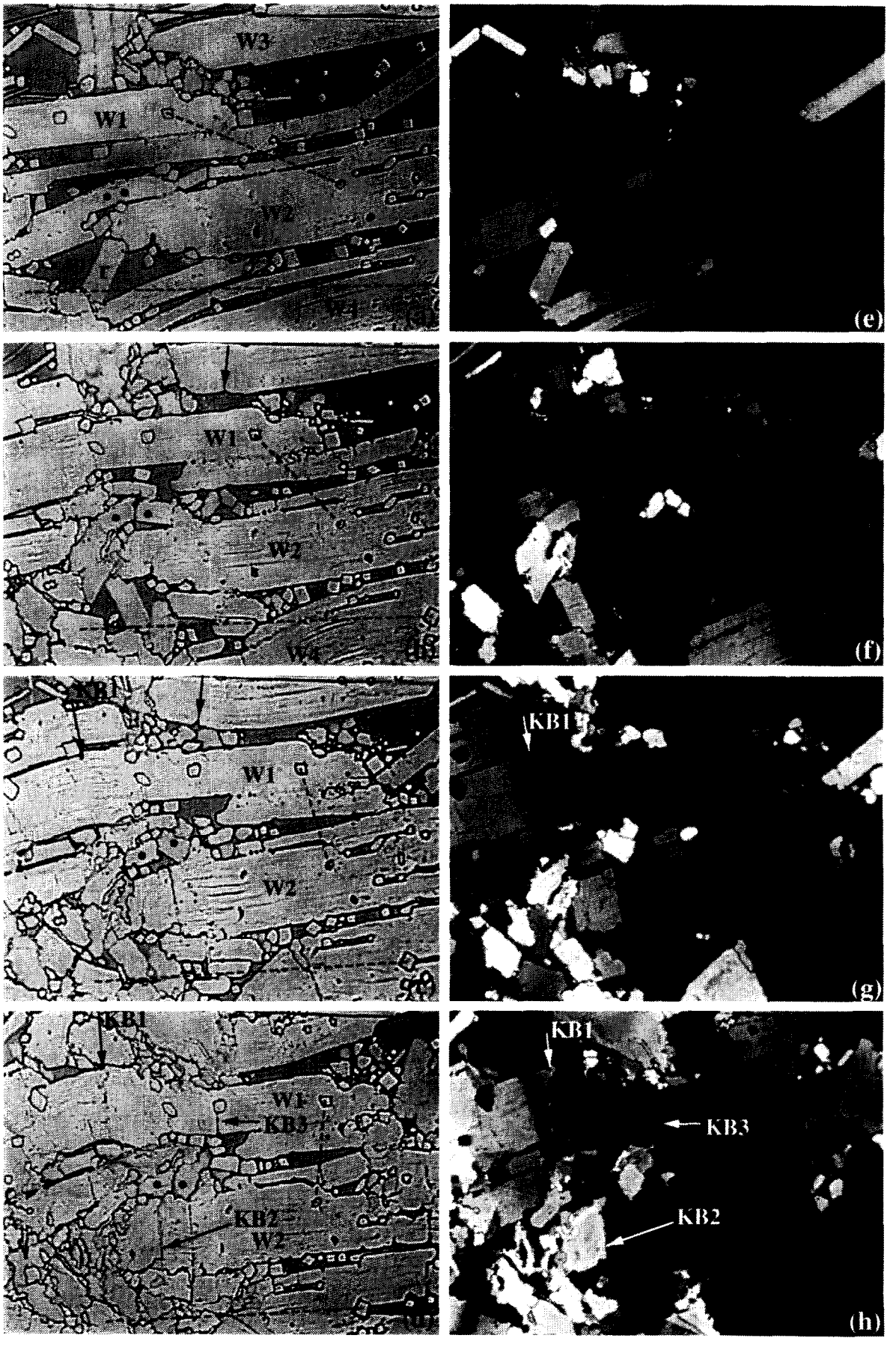

Fig. 2. Relatively fast, pure shearing deformation at 30°C, resulting in crystal plastic deformation and dynamic recrystallization of white phase (W). Cube phase (C), and melt (m) are also present. Sample strain rate: $3 \times 10^{-5}\ s^{-1}$; local strain rate (from lower dashed line): $1.8 \times 10^{-4}\ s^{-1}$. KB are kink boundaries, r marks crystal segments that have already been rotated by deformation prior to (a), by a process that can be followed further between the two black dots. Unlabelled arrows in (b) and (c) show cusp in crystal/melt interface. Plain light first column, crossed nicols second column. Time elapsed since (a)–(e) is 14 min in (b)–(f); 22 min in (c)–(g); 36 min in (d)–(h). Field width: 0.5 mm.

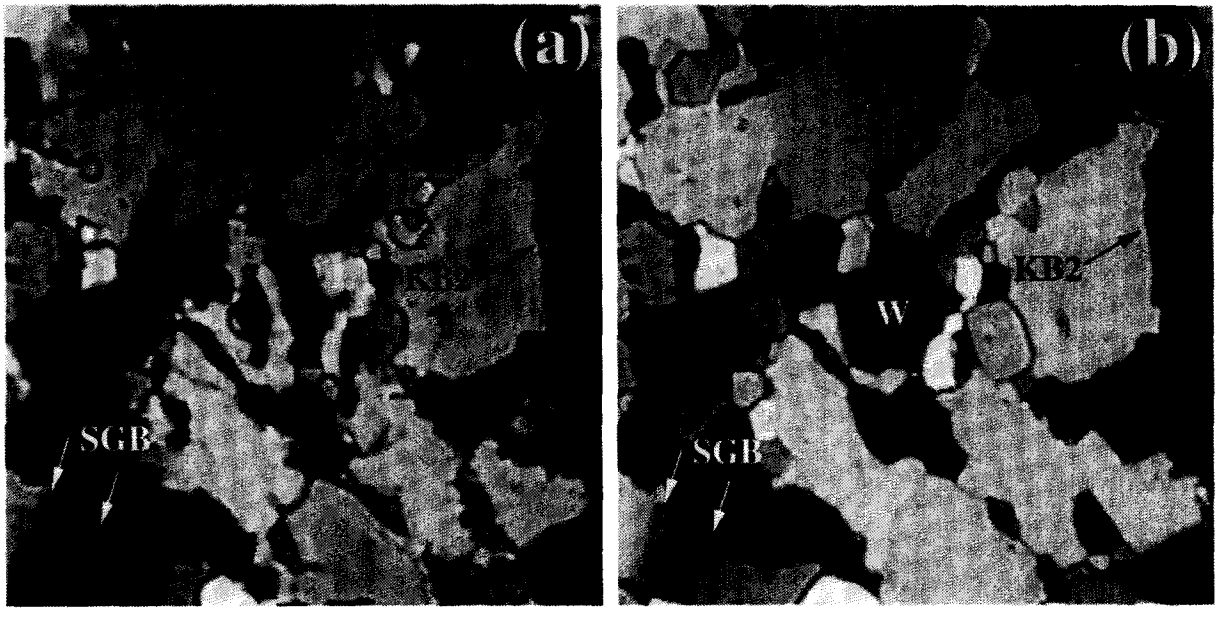

Fig. 3. Effects of static recovery at 30°C in the sample of Fig. 2. (a) Lower left corner of Fig. 2(h), at end of deformation. (b) Same area five days later. Grain boundaries have become more clearly defined, grain interiors less undulose. Some small grains have been eliminated, a few created. A large gray grain of the white phase (W) has grown. SGB are subgrain boundaries that have sharpened. KB 2 is kink boundary with same label in Fig. 2(h). Field width: 0.25 mm.

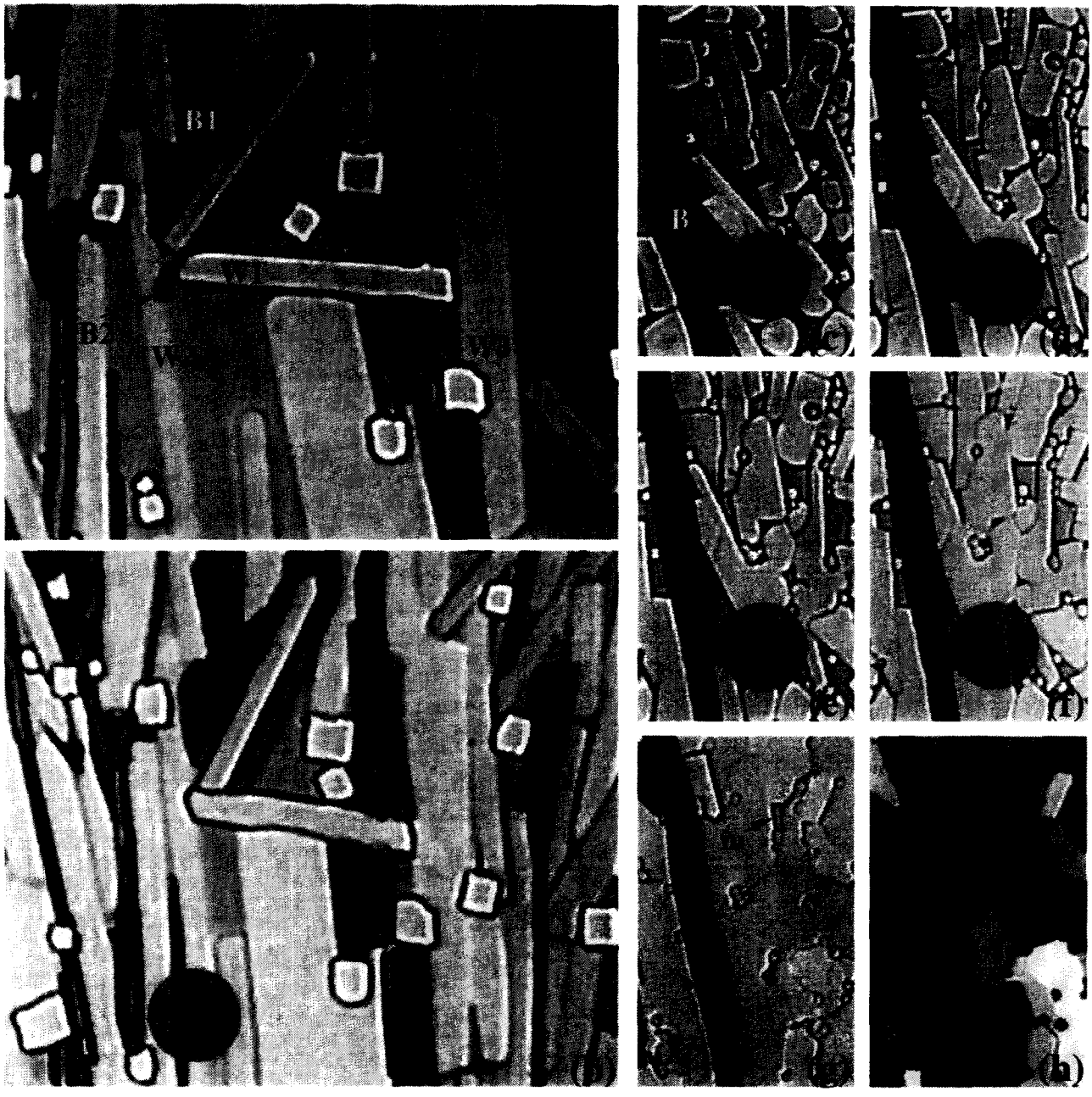

Fig. 4. Two relatively slow, pure shearing deformations, resulting in contact melting and filter pressing, at 27°C. Shortening direction is horizontal. White phase (W), blue phase (B), cube phase (C), and melt (m). (a)–(b) show incomplete filter pressing, sample strain rate: 3×10^{-6} s^{-1}; local strain rate (from spacing between W3 and white phase crystal under B2 label): 3.9×10^{-5} s^{-1}. Time elapsed: 111 min. Contact melting shortens W1 and also occurs in shaded circle. Field width: 0.3 mm. In (c)–(g), showing near-complete filter pressing, sample strain rate: 3×10^{-6} s^{-1}; local strain rate (from spacing between dots in (c) and (g)): 3×10^{-5} s^{-1}. Time elapsed since (c): 40, 60, 100, and 320 minutes by (d), (e), (f), and (g) respectively. Contact melting blunts lower point contact of W1 with B. Grain boundary migration assists sliding between W1 and W3 in shaded circle, by reorienting the sliding boundary between (d) and (e). Field width: 0.15mm. All images in plain light except (h), which is the crossed nicols equivalent of (g).

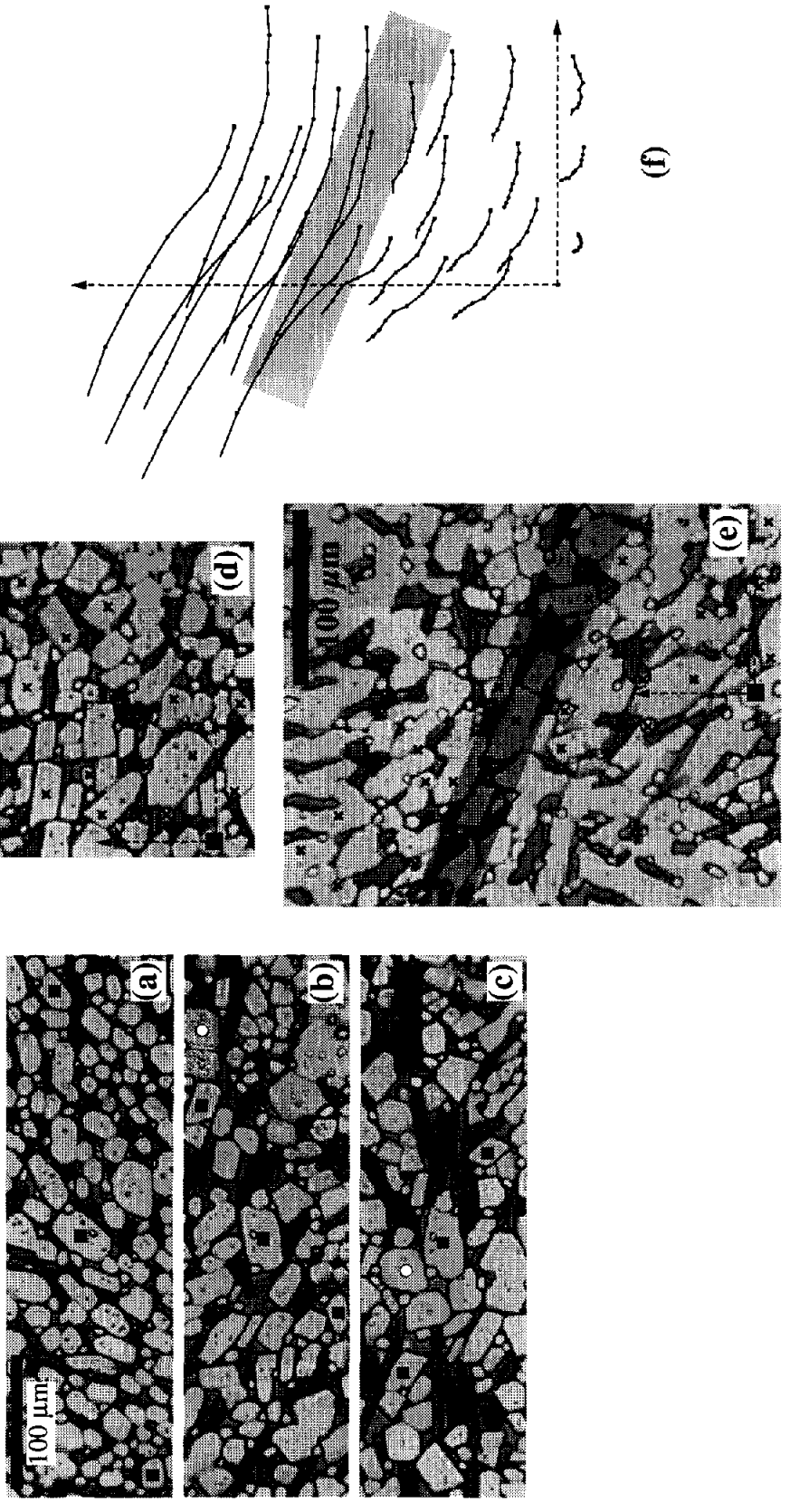

Fig. 5. Two sinistral shearing deformations accompanied by sliding of grain-past-grain and grain rotations. Sample shear strain rates: $3 \times 10^{-6}\ s^{-1}$, 40°C. In (a)–(c), local shear strain rate (from displacements of uppermost and lowermost grains marked with squares): $3.4 \times 10^{-4}\ s^{-1}$. The blue phase coarsens markedly. Time elapsed since (a): 210 and 340 minutes in (b) and (c) respectively. In (d)–(e), shearing is concentrated in a narrow zone occupying approximately the shaded region in (e). Within this zone, the local shear strain rate is $\sim 3.5 \times 10^{-4}\ s^{-1}$; x's mark the same material points in both images. Time elapsed between (d) and (e) is 120 min. (f) Shows trajectories of x's in (d) & (e) relative to an origin fixed to an arbitrary reference particle below the shear zone (squares in (d) and (e)) and axes parallel to the image edges. Spacing of dots along trajectories is proportional to particle velocities, and indicates a steep velocity gradient across the shear zone.

Table 1. Properties of phases in the experimental system

Phase	Chemical formula	Crystal symmetry	Color	Material property	Crystal form
Ammonium thiocyanate —'WHITE PHASE'	NH_4SCN	[a]Monoclinic	White	[a]Melting temperature at 1 atm = 149.6°C	Blocky to acicular
Diammonia tetrathiocyanato cobaltate —'BLUE PHASE'	$(NH_4)_2Co(NCS)_4 \cdot nH_2O$	[b]Tetragonal	Blue	[b]Melting temperature at 1 atm = ~150°C	Acicular
Ammonium chloride —'CUBE PHASE'	NH_4Cl	[a]Isometric	White	[a]Sublimates at 335°C, 1 atm	Blocky to square
Melt	Ionic compounds (e.g. NH_4^+) dissolved in water		Pale blue	[a]Diffusivity = $\sim 10^{-5}$ cm^2/s	

[a]From Handbook of Chemistry and Physics, 73rd edn (CRC Press).
[b]Inferred after observations.

same crystals at different stages. Based on this marker, the local shortening rate (38% in 2160 seconds) is 1.8×10^{-4}, or about six times the sample shortening rate. Although the bulk deformation is a pure shearing, an approximate simple shearing displacement pattern is observed locally in this field of view, as crystals W1 and W2 slide past each other. The upper dashed line indicates this large, local, dextral shearing movement. Nearby, there is a large, local, sinistral shearing, between crystal W1 and crystal W3 above it. This field of view exemplifies the principle that there can sometimes be little connection between the geometry and rates of local deformation on the scale of a few grains and the geometry and rates of bulk deformation on the scale of hundreds or thousands of grains.

Figure 2 also illustrates the familiar experience in synkinematic microscopy that the first images obtained (Figs. 2a & e) show the material *after* it has started to deform. (The camera was trained elsewhere at the start of the experiment, and was only moved to the area of Fig. 2 when interesting microstructural changes were noticed there.) The signs of deformation already in progress in Figs. 2(a & e) are rotated segments (r) of white phase crystals W1 and W2, and kink boundaries like the one near the left end of W3, which can be seen clearly in the crossed nicols image (Fig. 2e).

The two dots in crystal W2 mark a place where a melt-assisted(?), crystal plastic, segmentation process can be followed. In Fig. 2(e) it can be seen that there is a kink boundary at the site between the two dots in (a), with a small downward-pointing cusp in the upper crystal/melt interface where the kink boundary intersects the melt. In (b), relative rotation of the kink limbs has increased, and the boundary has become irregular, possibly indicating the presence of melt along the boundary, or grain boundary migration. In (c), misorientation is greater still, and some relative movement appears to have occurred parallel to the boundary. By this stage, the formerly continuous piece of W2 has been segmented into two effectively separate grains. Other indications of crystal plasticity in the white phase in Fig. 2 are the large kink boundaries (KB1,2,3) seen in (g) and (h), the more gradual lattice bending seen for example in W2 and W4 in (f), and the linear traces approximately bisected by the axial planes of these bends (e.g. in W4 in (b)–(f)) and by kink boundaries (e.g. KB1 in (c)–(g)). We interpret these linear traces as the traces of active slip planes, possibly etched out by the melt.

Cuspy boundaries like the one pointed out previously, with cusps pointing inwards toward the crystals, seem to be a characteristic feature of white phase crystals that are deforming plastically with melt present. A good example is seen at the unlabelled arrows in Figs. 2(b & c). The cusp between the two dots in (a) clearly marks the point of emergence of a kink boundary at the crystal/melt interface. But similar looking cusps can occur where there is no optical evidence of a kink boundary, or even of a subgrain boundary, for example just above the right hand dot in (a), and at the unlabelled arrows in (b) and (c). Such cusps may represent the former position of kink or subgrain boundaries that migrated away from the cusp site, too fast for the cusp to follow.

Local dynamic recrystallization by grain boundary migration is frequently observed, wherever solid–solid contacts are present, for example near the lower end of KB2, where an irregular boundary in Fig. 2(c) becomes more coarsely lobate in Fig. 2(d). Many examples are seen of rapid grain boundary migration in the fourteen-frame video movie from which the four frames of Fig. 2 were selected. The grain boundary migration is mostly too rapid to be resolved in the four images of Fig. 2.

Figure 3 shows microstructural changes in the lower left corner of Fig. 2(h) after static recovery for five days. Many small grains have been eliminated by grain boundary migration, and the same process has sharpened many of the grain boundaries, by straightening their traces, eliminating small grains along them, and perhaps by steepening their dips relative to the glass. This last process would eliminate some grain boundary surface area and energy. The large gray grain of the white phase (W) in Fig. 3(b) has been established by growth of one or both of the smaller gray grains visible in the center of Fig. 3(a). A small new grain has developed in Fig. 3(b), next to the B in the SGB label, from a subgrain in the same position in Fig. 3(a). Despite these adjustments in the grain boundary network, the large-scale intracrystalline microstructures induced by the deformation (KB2 and the subgrain boundaries in the lower left) remain visible, or even somewhat sharpened by the recovery

processes. The resultant microstructure seems to us to be indistinguishable from microstructure produced by dynamic recrystallization and partial recovery in material deformed entirely in the solid state.

Contact melting

The deformation process we call contact melting has been observed during low sample strain rate deformations, $\sim 10^{-6}$ per second, about an order of magnitude lower than the sample strain rate at which crystal plasticity is observed. (It may well also occur, however, in very slowly straining portions of our high sample strain rate samples, in areas we were not observing.) The term contact melting is used instead of the well established term pressure solution, since the mechanism of dissolution is not known and use of pressure solution may imply a mechanism in which the state of stress plays a direct role during dissolution (Sprunt & Nur 1977, Robin 1978). Another possible reason for dissolution where grains are pressed together is a solubility increase due to high defect density (Bosworth 1981, Lasaga 1981), i.e. 'strain solution'.

Strain accommodation by contact melting is shown in Figs. 4(a & b), where white phase crystal W1 shortens about 15% by melting at one or both of its points of contact with crystals W2, B2, and W3. W1 is bent slightly but there is not sufficient bending to account for the 15% shortening. Grain boundary migration from crystals W2 and W3 toward the center of crystal W1 can be ruled out as a mechanism for shortening W1, because the width of crystals W2 and W3 remains more or less constant.

Contact melting at phase boundaries (boundaries between two different solid phases) is also observed. Here it is typically asymmetrical, with melting mainly or wholly of only one of the phases in contact. For example, the white phase crystal W2 in Fig. 4(b) forms an indented boundary with two cube phase crystals in the shaded circle. This geometry suggests melting of the white phase crystal without comparable melting of the cube phase crystals. On the other side of these cube phase crystals, where they look truncated by a narrow blue phase crystal, the geometry suggests that the cube phase crystals have melted while the blue phase has undergone little or no melting. The sense of asymmetrical melting is not necessarily consistent however. The cube phase crystal immediately above W1 in (a) appears to have melted against W1 in (b), in contrast to the behavior earlier, where it was the white phase that appeared to melt at a white/cube boundary.

Another example of contact melting is shown in Figs. 4(c–h). The contacts between blue phase crystal B and white phase crystal W1 in Fig. 4(c) are two point contacts. The lower contact becomes wider as deformation progresses, by what we believe to be melting of W1 at the contact. There is also a faintly defined subgrain (?) within W1 near this proposed melting site which seems to be partly consumed by the melting. Note the conspicuous absence of bending of W1 into the melt pocket m. This suggests that the stress is too low in W1 for crystal plastic bending, of the kind seen in the higher strain rate sample of Fig. 2.

The dissolved constituents at contact melting sites should tend to raise the local concentration in the melt of the phase that is melting, above the equilibrium concentration. This may be expected to lead to crystallization or redeposition on free surfaces nearby, to maintain the equilibrium concentration. Such local redeposition is seen on white phase crystal W2 in Figs. 4(d & e).

In general, contact melting occurs at boundaries oriented at a high angle to the shortening direction. Although the mechanism of dissolution is not precisely known, this orientation of the melting boundaries suggests that high normal stress exists on these boundaries, which is related directly (through elastic strain energy) or indirectly (through plastic strain energy) to the melting.

Sliding on crystal boundaries

Sliding on the boundaries between crystals is active at all sample strain rates between $10^{-4.5}$ and 10^{-6} per second at 25 to 40° C. Where strain rate is high, sliding along crystal boundaries occurs with concurrent crystal plasticity, dynamic recrystallization and segmentation. When strain rate is low, and processes related to crystal plasticity do not occur, contact melting and grain boundary migration operate as an accommodation process and an assisting process for sliding, respectively. For example, grain boundary sliding occurs between crystals W1 and W3 between Figs. 4(c & d). Sliding on the grain boundary is accommodated (made possible geometrically) partly by contact melting of W1 at the B–W1 boundary and partly by rotation of W1. Grain boundary migration also *assists* (facilitates) sliding (in shaded circle in Figs. 4d–f). The original sliding boundary (between W1 and W3) changes its orientation by grain boundary migration (Figs. 4d & e), and further sliding then occurs on the grain boundary in the new orientation. Grain boundary migration assists horizontal shortening by sliding here, by providing a sliding surface that is better oriented than the original sliding boundary, for squeezing melt out of melt pocket m. Contact melting-accommodated sliding and grain boundary migration-assisted sliding allow large strains in the solid framework at stress levels below those needed for internal deformation of the crystals.

Sliding of grain-past-grain can also occur at higher strain rates in our material *without* concurrent crystal plasticity, where grain shapes are more equiaxed than in Figs. 1 and 3, such that grain interference effects are less severe. This is exemplified by the samples of Fig. 5, where although the sample strain rate is in the range we call low (3×10^{-6} s^{-1}), the local strain rates in the high strain rate zones are in the range we call high ($\sim 3 \times 10^{-4}$ s^{-1}).

FRAMEWORK SCALE DEFORMATION PROCESSES

Filter pressing

Filter pressing is the process by which interstitial melt in a solid framework is expelled through the framework during a volume decreasing deformation (McBirney 1984, p. 145). Filter pressing occurs in our experiments, when pure shearing grips were used, since use of such grips promotes deformation with volume decrease, on account of friction between the sample and the grips. During high sample strain rate experiments, filter pressing occurs by the combined processes of crystal plastic deformation and sliding along crystal boundaries, yielding microstructures (Figs. 2d & h) indistinguishable from those formed entirely in the solid state by plastic deformation, recrystallization and recovery processes. When the sample strain rate is low, filter pressing occurs by the combined processes of contact melting and sliding along crystal boundaries. An example of essentially complete filter pressing (to near-zero melt fraction) is provided by Figs. 4(g & h). It is a striking feature of this slowly and completely filter-pressed material that most of the grains in the final state are optically strain-free (Fig. 4h), and that no post-deformational recovery processes have been necessary to achieve this.

Grain flow, grain coarsening and a micro shear zone

In our samples with more equiaxed white phase crystals, deformed at low sample strain rates in shearing deformations, there is extensive grain-past-grain sliding and rolling but no fracturing of the white phase grains. This is the flow process termed *grain flow* by sedimentologists (see Carter 1975). Figures 5(a–c) show accumulation of shear strain of the order of 7 in a solid framework by grain flow at low melt fraction ($\sim 10\%$). Note the large rotation of the middle grain with a square ornament between Figs. 5(a & b), and its small backward rotation between Figs. 5(b & c). Note too the efficient changing of neighbors, that occurs in a flow like this. For example the grain marked with a white circle in Fig. 5(b), which is nowhere near the central grain with a square at this stage, becomes a nearest neighbor of the central grain by stage Fig. 5(c).

A surprising feature of the isothermal deformation of Figs. 5(a–c) is the coarsening that occurs during it. The white and cube phase crystals coarsen only slightly, but the blue phase coarsens markedly. This isothermal coarsening is evidently produced by syndeformational growth of some blue phase crystals, while others undergo contact melting and vanish. Syndeformational coarsening of the blue phase in this sample is described in greater detail in Park & Means (in press).

In some of our samples, grain boundary sliding was concentrated in very narrow shear zones only a few crystals wide. An example from a sample of low melt fraction is shown in Figs. 5(d–e). The particle trajectory map in Fig. 5(f) was constructed using material points in the crystals and shows the development of the narrow zone of concentrated sliding near the center of the field of view (shaded regions in Figs. 5(e & f)). It is noteworthy that this shear zone develops without conspicuously drawing the melt into the zone, or expelling melt from the zone. It is also remarkable that the shear zone (approximately the shaded region in Fig. 5(e)) looks so much like the surrounding less-sheared regions, texturally. Here there has been no obvious coarsening, perhaps because the shear strain is lower than in the material of Figs. 5(a–c). A cryptic kinematic domain of this kind would be difficult to recognize in rocks. The accumulated shear strain in the shear zone is of the order of 2 by stage Fig. 5(e). Above and below the shear zone, the shear strain of lines parallel to the zone is not zero, but it is distinctly lower than in the shear zone. So the shear zone is well-defined by the strain field even though it is cryptic texturally.

DISCUSSION

Petrographic recognition of melt-present deformation

Three main deformation processes at the crystal scale have been observed in the experiments: (1) crystal plastic deformation and dynamic recrystallization; (2) contact melting with or without local redeposition; and (3) sliding on crystal boundaries. Microstructures that may result from these processes in naturally deformed rocks are discussed below, using observations from our experiments and ideas already in literature.

If crystal plastic deformation occurred in crystals while melt was present and there had been no subsequent subsolidus deformation, the following microstructures could be expected if some melt remained when deformation ceased: (1) Deformed crystals surrounded by igneous mineral assemblages with pristine igneous textures (late stage 'pre-full crystallization fabrics' of Hutton 1988b); (2) Segmented or fractured and separated crystals with openings filled by igneous minerals (Hibbard 1987, Bouchez *et al.* 1992). If on the other hand the melt was fully crystallized before deformation ceased, or squeezed out before deformation ceased (as in Fig. 3a), then (1) and (2) would not be expected. (1) and (2) are therefore useful indicators of melt-present plastic deformation but their absence does not rule out such deformation.

When natural processes similar to our contact melting/redeposition are involved during deformation, the resulting microstructures may generally be cryptic. A possible exception is zoning truncated by grain boundaries. However, this microstructure can be formed by other processes, such as growth impingement and grain (or phase) boundary migration, so caution must be exercised. If these zone-truncating boundaries have a preferred orientation, the microstructures may be more reliable evidence of contact melting. Preferred orientation of indented boundaries may also be useful for recognition of contact melting.

A contrast can be predicted between the microstructural evidence for contact melting in a crystal–melt mixture and pressure solution in a subsolidus system. In the latter case, distinctive fibrous crystals or conspicuous grain overgrowths commonly (though not invariably) mark the 'sinks' where dissolved material is reprecipitated. In the case of contact melting/redeposition however, the 'sinks' are expected to be indistinguishable from any other growth site (e.g. W2 crystal in Figs. 4d & e). The 'sources' in contact melting may also be more cryptic than in the pressure solution situation. Pressure solution 'sources' are commonly either sutured or lined with insoluble phases. Both microstructures are conceivable at contact melting sites, though we have seen neither in our experiments. Sources may, therefore, be hard to identify in natural contact melting products and sinks will be impossible to identify, in contrast to subsolidus pressure solution products where both sources and sinks are prominent. Recognition of melt-present crystal boundary sliding in rocks will also be very difficult to recognize, since no microstructural signature need be left behind.

Petrographic recognition of filter pressing and grain flow

Two different types of filter pressing are observed in our experiments; (1) filter pressing which involves crystal plastic deformation with dynamic recrystallization, and (2) filter pressing which involves contact melting. In both types of filter pressing, the local modal mineralogy may be affected, since the melt that is removed should generally be of different composition from the framework crystals. If filter pressing occurs early enough during crystallization, a framework which consists of only one or two main phases may exist and a nearly monominerallic rock or two-phase adcumulate may be formed. If crystal plastic deformation and dynamic recrystallization occur during filter pressing, the resulting microstructure in the regions from which melt has been expelled will be similar to the microstructure formed in solid-state deformation. Layers of igneous rocks which show evidence of crystal plastic deformation neighbored by less deformed or undeformed comagmatic igneous layers may indicate filter pressing in a plastic deformation regime, if later solid-state deformation can be ruled out.

If more cryptic processes such as contact melting and grain boundary sliding are involved during filter pressing, the collapsed framework crystals may look undeformed, as shown in our low sample strain rate experiments (Figs. 4g & h). Undeformed-looking adcumulus is commonly associated with large mafic intrusions and petrologists have been working on the problem of how the interstitial melt is removed. Walker *et al.* (1988) explain the formation of adcumulus with a zone refining model in which diffusion under a thermal gradient is involved. Since the liquid phase is removed by continuous reequilibration between interstitial melt and the main reservoir of magma by diffusion (Walker *et al.* 1988), the resulting crystal boundaries in the cumulate will be growth impingement boundaries. However, when contact melting is involved during formation of adcumulus, the resulting crystal boundaries will be largely dissolution boundaries at which dissolution of one or both neighboring crystals occurred. Detailed petrographic work, including chemical imaging to see microstructures such as truncated zoning by grain or phase boundaries, may help to determine whether dissolution boundaries are present and whether filter pressing by contact melting contributed to the formation of adcumulus.

When a solid framework is deforming by grain flow, a shape preferred orientation may develop by rigid body rotation and tiling of crystals (Tikoff & Teyssier 1994). Preferred orientation of igneous minerals may be formed by rotation of crystals during grain flow even after formation of the solid framework, but since such shape preferred orientation is also possible by suspension flow or magmatic flow (Paterson *et al.* 1989), it is not a reliable criterion for grain flow at low melt fraction.

When a micro shear zone develops in a framework, recognition of such zones will be dependent on the volume change associated with the shearing deformation. When a micro shear zone develops without much change in the local melt fraction (Figs. 5d & e), the resulting microstructure may be cryptic. However, when the melt fraction increases or decreases in a shear zone, melt drawn into or expelled from the high strain zone will have different chemistry compared to the whole rock, and lead to narrow zones that are enriched or depleted in certain phases at equilibrium with the crystalline phases present in the neighboring region. Recognition of chemical equilibrium is important since a different mineral assemblage in such zones can also be formed by later igneous veining or dike injections.

How analogous to rock behavior is the experimental behavior?

For good analogy between the behavior of a material like ours and the behavior of some natural crystal/melt system, similar processes must act in both materials, and the relative *rates* of the processes must be similar instantaneously, and vary in a similar way over time. That is to say the 'mix' of processes, and its history, must be analogous to nature. Several of the processes seen in our material (crystal plasticity, grain boundary sliding, grain boundary migration) seem certain to be active in at least some naturally deforming crystal mushes, and contact melting may be too. Experiments on partially melted granitic rocks by Dell'Angelo *et al.* (1987) encountered some form of diffusion creep. However it is unclear how much this has in common with our contact melting process, where diffusive transfer of material is presumably through melt films at contact melting sites and then away from such sites through the bulk melt phase.

It is impossible at present to compare the rates of

active processes in our material and in natural crystal mushes, because the relative rates of various processes in nature are unknown. Nor are the relative rates of various processes accurately known in our experiments. All we have is the observation that there are at least two process-dominance fields in our material: a higher strain rate regime in pure shearing where stress in the white phase crystals rises high enough for extensive crystal plasticity, and a lower strain rate regime in pure shearing where contact melting and grain boundary sliding seem to be capable of keeping stress in the crystals below the threshhold for crystal plasticity. A material that shows changes in process-rate dominance like this, with changing experimental conditions, seems to us to have more chance of being analogous to nature in at least one of the fields than a material that displays no such switches. Figure 6 illustrates this idea. The first two bars show the rates of two processes (say straining by grain boundary sliding and straining by crystal plasticity) in some natural situation we wish to simulate. The bars at Fig. 6(a) show a perfectly scaled simulation, where each straining process is accelerated relative to nature by a factor of 10^7. But one does not know enough about nature or have enough control of the experimental process-rates to do this experiment overtly. Instead one tries two potential analog materials. In the material represented at Fig. 6(b), there is a switch in process-dominance over the range of available experimental conditions, with precise scaling to nature obtained at conditions somewhere between the middle and right hand pairs of bars. This material provides a good analog, at least at these conditions. The material repesented at Fig. 6(c) however is no good, because there is no switch in process dominance over the range of available experimental conditions, and it happens that the dominant process at all conditions is not the natural one (the black bar).

The simplest test of the relevance of our material's behavior to the behavior of rock systems in nature is simply to ask whether the textures seen in the experiments are like the textures of rocks. So far as we are aware, the answer is a guarded yes. Two reasons for caution are, as stated earlier, that different processes can in principle lead to rather similar-looking textures, and second, that the textures we see in the experiments to date are mostly melt-present textures (e.g. Figs. 1, 3a–f and 5), not melt-absent and somewhat recovered textures like the ones in rocks. So much more work on experimental texture-formation, along with more refined textural descriptions of rocks, is clearly necessary before the two sets of data can converge enough to shed conclusive new light on processes in natural crystal mushes.

CONCLUSIONS

We make the following suggestions for interpretation of rock textures based on experience to date.

(1) Igneous rocks free of crystal plastic deformation microstructures may nonetheless have undergone large deformations at low melt fractions. Some crystal–melt mixtures with solid frameworks can flow by contact melting/redeposition and grain boundary sliding, without crystal plastic deformation. Thus inferring deformation based on the presence of crystal plastic deformation microstructures, may be unreliable.

(2) When crystals in a framework with interstitial melt deform by crystal plasticity, the resulting microstructural characteristics may be similar to those formed by solid state crystal plasticity. However when deformation ceases before complete crystallization, the distinction may be easier, from assemblages of deformed crystals surrounded by igneous minerals with pristine igneous textures.

(3) The presence of microstructural features such as preferred orientation of boundaries that truncate chemical zonation, and preferred orientation of indented

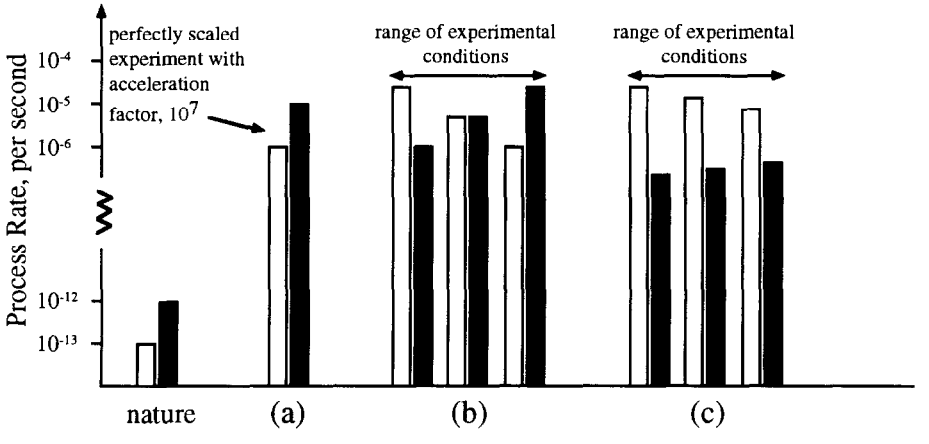

Fig. 6. Rates of processes (indicated by the height of bars) in nature and in analog experiments. (a) A perfectly scaled experiment, since the two process-rates in the experiment are accelerated by the same factor with respect to the corresponding process-rates in nature. (b) Experiments which show a change of process-dominance within the range of experimental conditions. In this situation, it is possible to achieve perfect scaling by adjusting the experimental conditions. (c) Experiments which do not show a change of process-dominance within the available range of conditions, and are not scaled to nature under any of these conditions.

boundaries may indicate contact melting in rocks and may be worth looking for in rocks.

(4) Complete removal of melt by filter pressing may be possible by crystal plastic deformation, contact melting, grain boundary sliding or a combination of these processes. Adcumulus may be formed by filter pressing during a sufficiently early stage of crystallization in magma, as also suggested by Sparks *et al.* (1985).

(5) Preferred orientation of euhedral igneous minerals may not always indicate suspension type flow. Such fabrics can perhaps also form during grain flow at low melt fraction (cf. Paterson *et al.* 1989).

(6) When a solid framework deforms by localized micro shear zones which do not draw melt in, recognition of the deformation process may be impossible. However, when such a zone draws melt in or expels melt during its development, a different mineral assemblage is likely to be present inside the zone. If the different mineral assemblage in such a zone is in chemical equilibrium with the bulk chemistry outside the zone, this may indicate development of high strain rate zones during melt-present deformation.

Acknowledgements—This work was supported by NSF grants EAR-9204781 (equipment), EAR-9017478 & EAR-9404872 to W. D. Means. We are much indebted to Ken Fowler and to Cees Van Staal for suggesting numerous improvements to the paper, and to Peter Hudleston for editorial assistance and patience.

REFERENCES

Bedard, J. H. 1991. Cumulate recycling and crustal evolution in the Bay of Islands ophiolite. *J. Geol.* **99**, 225–249.

Bosworth, W. 1981. Strain-induced preferential dissolution of halite *Tectonophysics* **78**, 509–525.

Bouchez, J. L., Delas, C., Gleizes, G., Nedelec, A. & Cuney, M. 1992. Submagmatic microfractures in granites. *Geology* **20**, 35–38.

Carter, R. M. 1975. A discussion and classification of subaqueous mass-transport with particular application to grain-flow, slurry flow, and fluxoturbidites. *Earth Sci. Rev.* **11**, 145–177.

Cooper, R. F. & Kohlstedt, D. L. 1986. Rheology and structure of olivine-basalt partial melts. *J. geophys. Res.* **91**, 9315–9323.

Dell'Angelo, L. N., Tullis, J. & Yund, R. A. 1987. Transition from dislocation creep to melt-enhanced diffusion creep in fine-grained granitic aggregates. *Tectonophysics* **139**, 325–332.

Hibbard, M. J. 1987. Deformation of incompletely crystallized magma systems: granitic gneisses and their tectonic implications. *J. Geol.* **95**, 543–561.

Hutton, D. H. W. 1988a. Igneous emplacement in a shear-zone termination: The biotite granite at Strontian, Scotland. *Bull. geol. Soc. Am.* **100**, 1392–1399.

Hutton, D. H. W. 1988b. Granite emplacement mechanisms and tectonic controls: inferences from deformation studies. *Trans. R. Soc. Edinb.* **79**, 245–255.

Karlstrom, K. E., Miller, C. F., Kingsbury, L. A. & Wooden, J. L. 1993. Pluton emplacement along an active ductile shear zone, Piute Mountains, southeastern California: Interaction between deformational and solidification processes. *Bull. geol. Soc. Am.* **105**, 213–230.

Lasaga, A. C. 1981. The atomistic basis of kinetics: defects in minerals. In: *Kinetics of Geochemical Processes* (edited by Lasaga, A. C. & Kirkpatrick, R. J.), *Reviews in Mineralogy, Mineral. Soc. Am.* **8**, 261–320.

McBirney, A. R. 1984. *Igneous Petrology*. Freeman, Cooper and Company, San Francisco.

Means, W. D. 1989. Synkinematic microscopy of transparent polycrystals *J. Struct. Geol.* **11**, 163–174.

Means, W. D. & Park, Y. 1994. New experimental approach to understanding igneous texture. *Geology* **22**, 323–326.

Nicolas, A. 1990. Melt extraction from mantle peridotites: hydrofracturing and porous flow, with consequences for oceanic ridge activity. In: *Magma Transport and Storage* (edited by Ryan, M. P.). John Wiley & Sons, Chichester, 159–173.

Park, Y. 1994. Microstructural evolution in crystal-melt systems. Unpublished Ph.D. Thesis. University at Albany, NY.

Park, Y. & Means, W. D., in press. Crystal rotation and growth during grain flow in a deforming crystal mush. In: *Evolution of Geologic Structures in Micro- and Macro-scales.* (edited by S. Sengupta) *The Ghosh/Naha Volume*. Chapman and Hall, London.

Paterson, S. R., Vernon, R. H. & Tobisch, O. T. 1989. A review of criteria for the identification of magmatic and tectonic foliations in granitoids. *J. Struct. Geol.* **11**, 349–363.

Robin, P-Y. F. 1978. Pressure solution at grain-to-grain contacts. *Geochim. cosmochim. Acta* **42**, 1383–1389..

Sparks, R. S. L, Huppert, H. E., Kerr, R. C., McKenzie, D. P. & Tait, S. R. 1985. Postcumulus processes in layered intrusions. *Geol. Mag.* **122**, 555–568.

Sprunt, E. S. & Nur, A. 1977. Experimental study of the effects of stress on solution rate. *J. geophys. Res.* **82**, 3013–3022.

Ten Brink, C. E. & Passchier, C. W. 1995. Modelling of mantled porphyroclasts using non-Newtonian rock analogue materials *J. Struct. Geol.* **17**, 131–146.

Tikoff, B. & Teyssier, C. 1994. Strain and fabric analyses based on porphyroclast interaction. *J. Struct. Geol.* **16**, 477–491.

Tobisch, O. T., Paterson, S. K., Saleeby, J. B. & Geary, E. E. 1989. Nature and timing of deformation in the Foothills terrane, central Sierra Nevada, California: its bearing on orogenesis. *Bull. geol. Soc. Am.* **101**, 401–413.

van der Molen, I. & Paterson, M. S. 1979. Experimental deformation of partially melted granite. *Contr. Miner. Petrol.* **70**, 299–318.

Walker, D., Jurewicz, S. & Watson, E. B. 1988. Adcumulus dunite growth in a laboratory thermal gradient. *Contr. Miner. Petrol.* **99**, 306–319.